



PERGAMON

International Journal of Plasticity

INTERNATIONAL JOURNAL OF

Plasticity

www.elsevier.com/locate/ijplas

A constitutive model for hcp materials deforming by slip and twinning: application to magnesium alloy AZ31B

A. Staroselsky^a, L. Anand^{b,*}^aUnited Technologies Research Center, MS 129-73 East Hartford, CT 06108, USA^bDepartment of Mechanical Engineering, Massachusetts Institute of Technology, Cambridge, MA 02139, USA

Received in revised form 14 January 2003

Abstract

A crystal-mechanics-based constitutive model, which accounts for both slip and twinning, has been developed for polycrystalline hcp materials. The model has been implemented in a finite-element program. The constitutive model is evaluated for the room-temperature deformation of the magnesium alloy AZ31B. By using comparisons between model predictions and macroscopically-measured stress-strain curves and texture evolution, we have deduced information about the dominant slip and twinning systems active at room temperature, and the values of the single-crystal parameters associated with slip and twin system deformation resistances. Our calculations show that the two main crystallographic mechanisms: (i) slip on basal $(0001) \langle 11\bar{2}0 \rangle$, prismatic $\{10\bar{1}0\} \langle 11\bar{2}0 \rangle$, and pyramidal $\{10\bar{1}1\} \langle 11\bar{2}0 \rangle$ systems, and (ii) twinning on pyramidal $\{10\bar{1}2\} \langle \bar{1}011 \rangle$ systems, play the dominant role in the deformation of magnesium at room temperature. However, to match the observed stress-strain curves, it is found necessary to account for non-crystallographic grain boundary related effects. We approximately account for these grain-boundary region accommodation effects by adding a suitably-weighted isotropic term to the flow rule. The isotropic plasticity term serves the important function of bounding the stress levels in the numerical calculations; it does not contribute to the crystallographic texture evolution. Overall, we show that a simple non-hardening crystal-mechanics-based constitutive model is able to reproduce the experimentally-measured stress-strain curves and crystallographic texture evolution in simple tension and compression on specimens made from an initially-textured rod, as well as plane strain compression experiments on specimens made from an initially-textured plate.

© 2003 Elsevier Science Ltd. All rights reserved.

Keywords: Twinning; Crystal plasticity; Finite elements; Mechanical testing

* Corresponding author. Tel.: +1-617-253-1635; fax: +1-617-258-8742.

E-mail address: anand@mit.edu (L. Anand).

1. Introduction

Deformation of hcp materials at low homologous temperatures typically occurs by crystallographic slip and deformation twinning occurring simultaneously, and the resulting mechanical properties are strongly affected by the interaction between these two major mechanisms of inelastic deformation. Unlike shear due to crystal-line slip, which typically takes place in either sense along a slip direction on a slip plane, the shear associated with twinning is typically polar in nature. This has a particularly important bearing on the mechanical response of many initially-textured polycrystalline hcp metals. For example, in extruded rods of most hexagonal metals the basal planes of the grains tend to be strongly aligned parallel to the axis of the rod. An important example is furnished by magnesium, for which it is well-known (e.g., Reed-Hill, 1973; Hosford, 1993) that a compressive stress applied nearly parallel to the basal planes favors twinning, whereas a similarly-directed tensile stress cannot induce such twins. As a consequence, the stress-strain curves in tension and compression obtained from specimens made from extruded magnesium rods are very different (see Fig. 6 of Reed-Hill, 1973). In compression, yielding occurs at a stress level which is almost half that in tension. This strong tension-compression asymmetry strongly influences the use of magnesium and many of its alloys as structural members, such as beams, since the compressive side of a beam will plastically deform long before the tensile side does.

Unlike the recent progress in the formulation, numerical implementation, and verification of a mathematical theory of crystal plasticity for fcc and bcc metals deforming by crystallographic slip (e.g., Anand et al., 1997, Dawson and Marin, 1998, Kothari and Anand, 1998, Balasubramanian and Anand, 2002), the modeling of plastic deformation due to slip and twinning is less well developed. Some of the early considerations for fcc materials are those of Chin et al. (1969), and Chin and Mammel (1970); for a brief review of this early work on twinning, see Chin (1975). Subsequently, important contributions were made by Van-Houtte (1978) and Tome et al. (1991). For recent finite-deformation crystal-mechanics-based models for plastic deformation of fcc materials by slip and twinning, see Staroselsky and Anand (1998a, b), Kalidindi (1998, 2001), Myagchilov and Dawson (1999)¹ and Schoenfeld and Kad (2002).²

The purpose of this paper is to develop a constitutive model for polycrystalline hcp materials. For the experimental validation of the model, we have focussed our attention on the response of an initially-textured magnesium alloy AZ31B (96.486% Mg, 2.798% Al, 0.715% Zn, Balance, Mn, Fe) deforming by crystallographic slip and twinning at room temperature. Briefly, we find that the two main crystallographic mechanisms (i) slip on basal (0001) $\langle 11\bar{2}0 \rangle$, prismatic $\{10\bar{1}0\}$ $\langle 11\bar{2}20 \rangle$, and pyramidal $\{10\bar{1}0\}$ $\langle 11\bar{2}0 \rangle$ systems (Fig. 1), and (ii) twinning on pyramidal $\{10\bar{1}2\}$

¹ These authors have also considered twinning in hcp materials, but they concentrated their attention on texture evolution; no simulation of stress-strain curves and comparisons against experiments was attempted.

² These authors considered twinning in titanium alloys, but they considered only an idealized two-dimensional model for the slip and twinning systems; again, no simulation of stress-strain curves and comparisons against experiments was attempted.

$\langle\bar{1}011\rangle$, are insufficient to accommodate all possible imposed deformations on polycrystalline aggregates. It appears that phenomena related to relative sliding and separation between neighboring grains become important. To match the observed stress–strain curves, we approximately account for these grain-boundary region accommodation effects by adding a suitably-weighted isotropic term to the flow rule. The isotropic plasticity term serves the important function of bounding the stress levels in the numerical calculations; it does not contribute to the crystallographic texture evolution.

The plan of the paper is as follows. In Section 2 we briefly review the mechanisms of inelastic deformation in hcp metals. In Section 3 we present our constitutive model to represent the behavior of polycrystalline hcp materials at low homologous temperatures. The application of the model to the polycrystalline magnesium alloy AZ31B is discussed in Section 4, where we show the results of experiments and corresponding numerical simulations for the stress–strain response and texture evolution in a few different modes of deformation. We close in Section 5 with some final remarks.

2. Intragranular and intergranular deformation mechanisms in polycrystalline hcp metals

2.1. Intragranular mechanisms

The directions for easy crystallographic slip in hcp single crystals are the three $\langle 11\bar{2}0 \rangle$ or $\langle a \rangle$ closed-packed directions. At low homologous temperatures, the three dominant sets of planes which contain this slip direction are (i) the (0001) basal plane, (ii) the three $\{10\bar{1}0\}$ prismatic planes, and (iii) the six $\{10\bar{1}1\}$ pyramidal planes; see Fig. 1. Crystallographic slip in hcp single crystals is commonly observed to occur on the basal- $\langle a \rangle$ or prismatic- $\langle a \rangle$ systems. The activation of pyramidal slip systems in polycrystalline aggregates occurs primarily due to the large stresses generated in grain-boundary regions because of the misorientation between neighboring grains (e.g., Burke and Hibbard, 1952; Raynor, 1959).

All the easy $\langle 11\bar{2}0 \rangle$ slip directions are perpendicular to the c -axis, and therefore slip on the systems listed above does not produce any elongation or shortening parallel to the c -axis. In order to accommodate straining in the c -direction, slip or twin systems with $\langle \alpha c + \beta a \rangle$ slip/twin directions must be operative. At low homologous temperatures,³ *deformation twinning* is the dominant mechanism which allows for inelastic shape changes in the c -direction.

In the standard local description of a twinned crystal (e.g., Kelly and Groves, 1970; Pitteri, 1985, 1986; Zanzotto, 1996), we have two regions \mathcal{R}_1 and \mathcal{R}_2 which are separated by a plane \mathcal{I} with unit normal $\hat{\mathbf{n}}$ pointing into \mathcal{R}_2 . The deformation in

³ At high homologous temperatures, slip in the $\langle 11\bar{2}3 \rangle$ directions becomes possible, and the slip planes containing this slip direction are the first-order pyramidal $\{10\bar{1}1\}$ and the second-order pyramidal $\{11\bar{2}2\}$ planes.

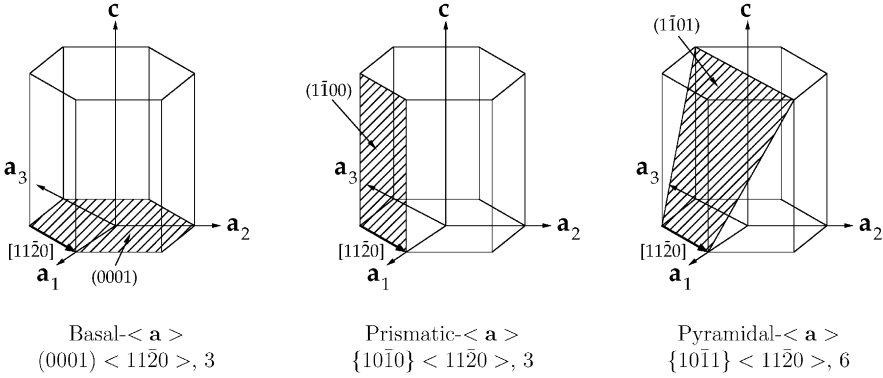


Fig. 1. Basal- $\langle a \rangle$, prismatic- $\langle a \rangle$, and pyramidal- $\langle a \rangle$ slip systems in hcp materials.

each region is homogeneous, and continuous across the interface. Then, at the macroscopic level,

- The constant deformation gradients \mathbf{F}_1 and \mathbf{F}_2 in the two regions, satisfy

$$\mathbf{F}_2 = \mathbf{S}\mathbf{F}_1,$$

where

$$\mathbf{S} = \mathbf{1} + \mathbf{a} \otimes \hat{\mathbf{n}}, \quad \mathbf{a} \cdot \hat{\mathbf{n}} = 0$$

is a simple shear. Since we can always choose one of the two “phases” of the twin as an undistorted reference, it is usual to select $\mathbf{F}_1 = \mathbf{1}$.

Further, at the molecular level, the crystal lattices in \mathcal{R}_2 and \mathcal{R}_1 satisfy the following:

- The lattice in \mathcal{R}_2 can be obtained by the simple shear \mathbf{S} of the lattice⁴ \mathcal{R}_1 .
- The lattice in \mathcal{R}_2 can be obtained by a rotation or a reflection \mathbf{R}^{tw} of the lattice in \mathcal{R}_1 .

The twinning shear $\mathbf{S} = \mathbf{1} + \mathbf{a} \otimes \hat{\mathbf{n}}$, may be written as

$$\mathbf{S} = \mathbf{1} + \gamma_0 \hat{\mathbf{m}} \otimes \hat{\mathbf{n}}, \quad \text{where } \gamma_0 = |\mathbf{a}|, \quad \text{and } \hat{\mathbf{m}} = \frac{\mathbf{a}}{|\mathbf{a}|}. \quad (1)$$

The plane orthogonal to the unit vector $\hat{\mathbf{n}}$ is the interface \mathcal{I} of the twin. The unit vector $\hat{\mathbf{m}}$ denotes the “direction of twinning shear,” γ_0 is the “amount of twinning shear,” and $\mathbf{a} = \gamma_0 \hat{\mathbf{m}}$ is the “shear amplitude vector.” The plane S which contains $\hat{\mathbf{m}}$ and $\hat{\mathbf{n}}$ is the “plane of shear.” Classically, macroscopic twinning shears are specified

⁴ In many cases the description of twinning in terms of a simple shear of the lattice works only for some of the atoms of the twinned crystal; additional “shuffle” displacements are usually necessary for the remaining atoms.

by four quantities $\{K_1, K_2, \eta_1, \eta_2\}$, called the “twinning elements”.⁵ K_1 is the interface of the twin, the plane orthogonal to $\hat{\mathbf{n}}$, and is called the “first undistorted plane” of the shear. The direction η_1 is parallel to the direction of shear $\hat{\mathbf{m}}$. It is easy to show that a vector parallel to a direction η_2 in S will be of the same length after the shear has been applied, if the angle α that it makes with $\hat{\mathbf{n}}$ is given by $\gamma_0 = 2 \tan \alpha$. Clearly, all vectors in the plane through η_2 which is normal to S are unchanged in length, although rotated; this plane is labelled K_2 , and is called the “second undistorted plane.” Thus, K_2 is the unique plane which is only rotated by the simple shear, and η_2 indicates the line of intersection of the planes S and K_2 . Note that η_2 is parallel to $(2\hat{\mathbf{n}}-\mathbf{a})$, and that K_2 is the plane containing $(2\hat{\mathbf{n}}-\mathbf{a})$ and $\hat{\mathbf{n}} \times \mathbf{a}$. The directions η_1 and η_2 are usually oriented as \mathbf{a} and $(2\hat{\mathbf{n}}-\mathbf{a})$, respectively.

There are three ways that a crystal lattice can be sheared while still retaining its crystal structure and symmetry: (i) When (K_1, η_2) are rational, while (K_2, η_1) are irrational; such a twinning mode is called a type-1 twin. (ii) When (K_2, η_1) are rational, while (K_1, η_2) are irrational; such a twinning mode is called a type-2 twin. (iii) When all four elements $\{K_1, K_2, \eta_1, \eta_2\}$ are rational; in this case the twin is called a “compound” twin.

Materials with closed-packed hexagonal lattices exhibit many types of twinning; however, for all hexagonal metals at low homologous temperatures, deformation twinning on $\{10\bar{1}2\}$ planes is the dominant mechanism which allows for inelastic shape changes in the c -direction. The full description of the $\{10\bar{1}2\}$ deformation twinning mode is (e.g., Hosford, 1993; Christian and Mahajan, 1995):

$$K_1 = \{10\bar{1}2\}, \quad K_2 = \{\bar{1}012\}, \quad \eta_1 = \langle \bar{1}011 \rangle, \quad \eta_2 = \langle \bar{1}01\bar{1} \rangle, \quad (2)$$

$$S = \{1\bar{2}10\}, \quad \gamma_0 = \frac{\sqrt{3}}{(c/a)} - \frac{(c/a)}{\sqrt{3}} \quad (3)$$

The amount of shear associated with twinning depends on the c/a ratio, where a denotes the interatomic distance on the (0001) basal plane in any of the three basal closed-packed $\langle 11\bar{2}0 \rangle$ directions, and c is the height of the unit cell in the c -direction.⁶ Such a twinning system is schematically shown in Fig. 2a. For materials with $c/a < \sqrt{3}$ the direction of shear is $[\bar{1}011]$, and twinning occurs under tension parallel to the c axis. For materials with $c/a > \sqrt{3}$ the direction of shear is $[10\bar{1}\bar{1}]$, and twinning occurs under compression parallel to the c axis.

⁵ The shear \mathbf{S} is fully specified by $\{\gamma_0, \hat{\mathbf{m}}, \hat{\mathbf{n}}\}$; it is also fully determined by the pair (K_1, η_2) , or by the pair (K_2, η_1) . Thus, if (K_1, η_2) are known, then $\hat{\mathbf{n}}$ is known, the unit vector \mathbf{g} in the direction η_2 is known, the amount of shear is given by $\gamma_0 = 2 [(\mathbf{g} \cdot \hat{\mathbf{n}} - 1)]^{1/2}$, and the direction of shear is given by $\hat{\mathbf{m}} = 2\gamma_0^{-1}[\hat{\mathbf{n}} - (\mathbf{g} \cdot \hat{\mathbf{n}})^{-1}\mathbf{g}]$. Thus a shear is determined by either the pair (K_1, η_2) or (K_2, η_1) , of its elements, and the macroscopic shear \mathbf{S} is typically given by means of crystallographic indices of such elements.

⁶ The ideal c/a ratio, calculated on the basis of a hard sphere model, is $\sqrt{8/3} = 1.633$. However, in real materials it varies from 1.567 for beryllium to 1.886 for cadmium. For magnesium, $c/a = 1.624$, which is close to the ideal value.

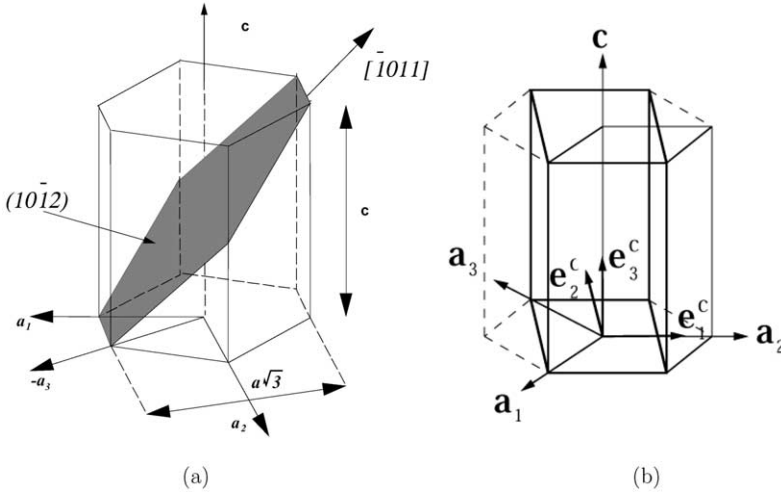


Fig. 2. (a) The $\{10\bar{1}2\}$ $[\bar{1}011]$ tensile twinning system for magnesium. (b) Orthonormal system $\{e_i^c | i = 1, 2, 3\}$ used to describe slip and twinning systems.

Note that since the elements $\{K_1, K_2, \eta_1, \eta_2\}$ for the $\{10\bar{1}2\}$ twinning mode are all rational, such twins are of the compound type. For compound twins, the orientation relation between the twin and the parent may be described by the rotation

$$\mathbf{R}^{tw} = -\mathbf{1} + 2\hat{\mathbf{n}} \otimes \hat{\mathbf{n}}. \quad (4)$$

For later use, we note the four coordinate axes, $\{\mathbf{a}_1, \mathbf{a}_2, \mathbf{a}_3, \mathbf{c}\}$, Miller–Bravais system is not convenient for numerical modeling, because the vectors $\{\mathbf{a}_1, \mathbf{a}_2, \mathbf{a}_3\}$ are not linearly independent. For this purpose, we construct an orthonormal basis $\{\mathbf{e}_1^c, \mathbf{e}_2^c, \mathbf{e}_3^c\}$ such that the \mathbf{e}_1^c -axis is the $[\bar{1}2\bar{1}0]$ -direction; \mathbf{e}_2^c -axis is the $[\bar{1}010]$ -direction, and the \mathbf{e}_3^c -axis is the $[0001]$ -direction; see, Fig. 2b. Let \mathbf{n}_0 denote a slip/twin plane normal in the reference configuration, and \mathbf{m}_0 denote a slip/twin plane direction in the reference configuration. We use slip and twin systems described by $(\mathbf{m}_0, \mathbf{n}_0)$ in our calculations. The tabulated components of the potential slip and twinning systems $(\mathbf{m}_0^i, \mathbf{n}_0^i)$, with respect to the orthonormal basis $\{\mathbf{e}_i^c | i = 1, 2, 3\}$, for hcp materials at room temperature may be found in Staroselsky (1998).

2.2. Intergranular mechanisms

In polycrystalline magnesium alloys, inelastic deformation originates from both intragranular slip and twinning modes of deformation, as well as some intergranular deformation modes. It appears that phenomena related to relative sliding and separation between neighboring grains become important. The most important intergranular mechanism of inelastic deformation is grain boundary sliding as shown in Fig. 3, taken from Hauser et al. (1955). An examination of the deformation of the fiduciary lines in this photograph clearly shows shear displacements across grain boundaries, and these occur at relatively low macroscopic strain levels.

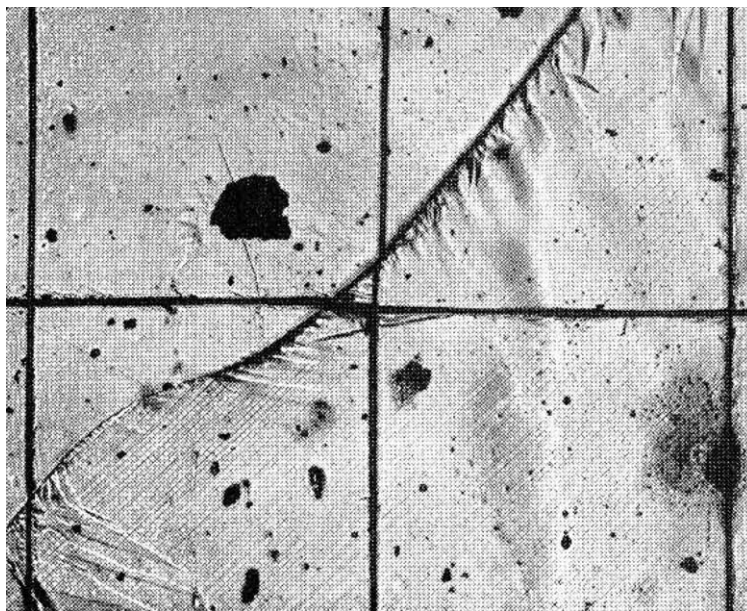


Fig. 3. Optical micrograph revealing grain boundary sliding in magnesium; after Hauser et al. (1955).

They have observed that the volume fraction ξ of a grain affected by these intergranular mechanisms is small, $\xi \ll 1$, and that the intergranular grain boundary accommodation effects in neighboring grains occur in thin layers around their mutual grain boundary. Such non-crystallographic effects cause stress relaxation, and as we shall see, it is important to account for these effects in a constitutive model in order to match the macroscopic stress–strain curves.

3. Constitutive equations

The overall plastic deformation of a crystal is always inhomogeneous at length scales associated with slip and twinning, and should be defined as an average over a volume element that must contain enough dislocation loops and twins to result in an acceptably smooth process at the continuum level of interest here. The smallest such volume element above which the plastic response can be considered smooth, is labeled a representative-volume element. In our model we will not account for the fine spatial structure of dislocation loops, slip bands and twin lamella in a crystal, as well as the inherently non-uniform deformation that typically occurs in the vicinity of grain boundaries, and we shall take a whole crystal as a representative-volume element (RVE). In particular, for later use, we denote the volume fraction of twins corresponding to the i th twin system in a RVE by $f^i \geq 0$, with $\sum_i f^i \leq 1$. Also, we assume that there is no de-twinning, and require that $f^i \geq 0$.

The two major kinematic issues in modeling twinning are: (i) accounting for the shear associated with twinning; and (ii) accounting for the reorientation of the crystal lattice due to twinning. Van-Houtte (1978) appears to have been the first to propose a simple tractable scheme for reorientation due to twinning. In his approach, if a grain twins, then the shear due to twinning is first accumulated as a pseudo-slip; that is, the shearing rate on the twin systems is taken to be given by $\dot{\gamma}^i = \dot{f}^i \gamma_0$, where γ_0 is the amount of twinning shear, and the crystal lattice is given the twinning-related orientation only if a probabilistic criterion, based on the relative volume fractions of the twinned and non-twinned parts of a crystal, is met. We shall employ Van-Houtte's approach to account for the twinning shear as well as the lattice reorientation due to twinning.

We will employ the constitutive model of Staroselsky and Anand (1998a) for deformation of a single crystal by combined slip and twinning, and modify it to *approximately account* for the grain-boundary accommodation effects discussed earlier. The governing variables in the constitutive model are taken as: (i) The Cauchy stress, \mathbf{T} . (ii) The deformation gradient, \mathbf{F} . (iii) Crystal slip and twin systems labeled by integers i . Each system is specified by a unit normal \mathbf{n}_0^i to the slip/twin plane, and a unit vector \mathbf{m}_0^i denoting the slip/twin direction. The slip and twin systems $(\mathbf{n}_0^i, \mathbf{m}_0^i)$ are assumed to be known in the reference configuration. The amount of shear, γ_0 , and the lattice rotation accompanying twinning, \mathbf{R}^{tw} , are also assumed to be known. (iv) A plastic deformation gradient, \mathbf{F}^p , with $\det \mathbf{F}^p = 1$. This represents the cumulative effect of dislocation motion and shear due to twinning on the active slip and twin systems in the crystal; it also accounts for the grain boundary accommodation effects in an approximate volume-averaged sense. (v) The slip and twin system deformation resistances $s^i > 0$, with units of stress. (vi) The twin fractions $f^i \geq 0$.

The elastic deformation gradient is defined by⁷ $\mathbf{F}^e \equiv \mathbf{F} \mathbf{F}^{p-1}$ with $\det \mathbf{F}^e > 0$, and it describes the elastic distortion of the lattice; it is this distortion that gives rise to the stress \mathbf{T} .

Next, let $\bar{\mathbf{S}}_0 = (\det \mathbf{F}) \mathbf{T} \mathbf{F}^{-T}$ denote the first Piola–Kirchhoff stress. Then, the stress power per unit reference volume is $\dot{\omega} = \bar{\mathbf{S}}_0 \cdot \dot{\mathbf{F}}$, which, since $\det \mathbf{F}^p = 1$, is also equal to the stress power per unit volume of the relaxed configuration determined by \mathbf{F}^p . This stress power may be additively decomposed as $\dot{\omega} = \dot{\omega}^e + \dot{\omega}^p$, where $\dot{\omega}^e = \mathbf{T}^e \cdot \dot{\mathbf{E}}^e$ is the elastic stress power per unit volume of the relaxed configuration, with

$$\mathbf{E}^e \equiv (1/2) \{ \mathbf{F}^{eT} \mathbf{F}^e - 1 \} \quad \text{and} \quad \mathbf{T}^e \equiv (\det \mathbf{F}^e) \mathbf{F}^{e-1} \mathbf{T} \mathbf{F}^{e-T}, \quad (5)$$

the Green elastic strain measure and the symmetric second Piola–Kirchhoff stress tensor relative to the relaxed configuration, respectively, and

$$\dot{\omega}^p = (\mathbf{C}^e \mathbf{T}^e) \cdot \left(\dot{\mathbf{F}}^p \mathbf{F}^{p-1} \right), \quad \mathbf{C}^e \equiv \mathbf{F}^{eT} \mathbf{F}^e, \quad (6)$$

is the plastic stress power per unit volume of the relaxed configuration.

⁷ The decomposition of \mathbf{F} into a plastic part \mathbf{F}^p and an elastic part \mathbf{F}^e is due to Kröner and Lee (Kroner, 1960; Lee, 1969).

3.1. Constitutive equation for stress

Elastic stretches in metallic single crystals are generally small. Accordingly, the constitutive equation for the stress in a metallic single crystal is taken as the linear relation

$$\mathbf{T}^e = \mathcal{C}[\mathbf{E}^e], \quad (7)$$

where \mathcal{C} is a fourth-order anisotropic elasticity tensor, where \mathbf{E}^e and \mathbf{T}^e are the strain and stress measures defined in Eq. (5).

3.2. Slip and twinning conditions

Let

$$\mathbf{S}_0^i = \mathbf{m}_o^i \otimes \mathbf{n}_o^i \quad (8)$$

denote the Schmid tensors and, consistent with Eq. (6), let

$$\mathbf{T}^i = (\mathbf{C}^e \mathbf{T}^e) \cdot \mathbf{S}_0^i \quad (9)$$

denote the resolved shear stress on the i th slip/twin system. Then, the conditions for slip and twinning are taken as

$$\phi^i = |\tau^i| - s^i \leq 0 \quad (10)$$

where s^i are the slip and twin system deformation resistances.

3.3. Flow rule

The evolution of the plastic deformation gradient due to crystallographic slip and twinning is given by

$$\dot{\mathbf{F}}^p = \mathbf{L}^p \mathbf{F}^p, \quad (11)$$

with \mathbf{L}^p given by the sum of the shearing rates on all the slip and twin systems (Staroselsky and Anand, 1998a)

$$\mathbf{L}^p = \sum_i \dot{\gamma}^i \text{sign}(\tau^i) \mathbf{S}_0^i, \quad (12)$$

and the shearing rates are restricted as follows:

$$\dot{\gamma}^i \geq 0, \quad \text{and} \quad \dot{\gamma}^i \phi^i = 0. \quad (13)$$

This flow rule needs to be modified to account for grain boundary accommodation effects. Since most non-crystallographic effects are localized around grain boundaries, as an approximation we imagine a ‘‘grain boundary layer’’ of volume fraction $\xi \ll 1$ which deforms in accordance with a simple isotropic plasticity type flow rule, while the rest of the crystal, with volume fraction $(1-\xi)$, deforms according to crystal plasticity theory. That is, we take the flow rule to be given by

$$\mathbf{L}^p = (1 - \xi) \sum_i \dot{\gamma}^i \text{sign}(\tau^i) \mathbf{S}_0^i + \xi \mathbf{M}, \quad (14)$$

$$\mathbf{M} = \dot{\epsilon}_0 \left\{ \frac{\bar{\sigma} - s_{th}}{s} \right\}^{\frac{1}{m}} \left(\frac{3\mathbf{T}e'}{2\bar{\sigma}} \right), \quad (15)$$

$$\bar{\sigma} = \sqrt{(3/2)\mathbf{T}e' \cdot \mathbf{T}e'}, \quad (16)$$

$$\xi = \begin{cases} 0 & \text{if } \bar{\sigma} \leq s_{th}, \\ > 0 & \text{if } \bar{\sigma} > s_{th}. \end{cases} \quad (17)$$

Here, s is an internal variable, with a threshold value s_{th} . The “isotropic term” is activated only if the equivalent tensile stress $\bar{\sigma}$ in a grain exceeds this threshold.

Note that while we have modeled slip and twinning as rate-independent, for reasons of computational convenience the grain boundary accommodation term is modeled as rate-dependent with a small value for the rate sensitivity parameter m .

The primary purpose of introducing the isotropic plasticity term is to bound the stress levels in our numerical calculations; without such a term, the assumption of perfectly bonded grains leads to unrealistically high stress levels. This term does not contribute to the crystallographic texture evolution. We recognize that the method proposed here is perhaps not the best way to account for the grain-boundary sliding/decohesion related phenomena. However, at this point we find it to be a computationally effective way to estimate the macroscopic averaged stress–strain response. A more detailed study would involve providing separate traction-separation constitutive relations for the grain- boundary response, but such work is still in its infancy.

3.4. Evolution equations for slip and twin resistances

These may be generically written to be given by $\dot{s}^i = \sum_j h^{ij} \dot{\gamma}^j$, where h^{ij} are the hardening moduli. However, in our calculations we shall use the simple, non-hardening assumption; that is, we shall set $h^{ij} = 0$. Also, the resistance s appearing in the isotropic term in the flow rule, Eq. (15), will be taken to be a constant.

3.5. Consistency conditions

During plastic flow the following consistency conditions must be satisfied:

$$\dot{\gamma}^i \phi^i = 0 \text{ if } \phi^i = 0. \quad (18)$$

The consistency conditions serve to determine the shearing rates $\dot{\gamma} \geq 0$ on the slip and twin systems.

3.6. Evolution equations for twin volume fractions

For the twin systems,

$$\dot{f}^i = \dot{\gamma}^i / \gamma_0 \geq 0, \quad (19)$$

where γ_0 is the twinning shear.

3.7. Lattice reorientation condition

Let f denote the volume fraction of the twin system with the maximum value of f^i at a given time t , and let a random number $\zeta \in [0.3, 1]$ denote a representative maximum value of f in a RVE. The lattice reorientation condition suggested by Van Houtte (1978), and adopted here, is that if $f > \zeta$, then the orientation of the RVE be replaced by the twin related orientation, and f^i be reinitialized to zero. That is, if $\{e_i^c | i = 1, 2, 3\}$ denotes a local orthonormal basis associated with the crystal lattice in the old relaxed configuration, then once this criterion is met the crystal basis in the new relaxed configuration of the crystal be taken as $e_i^{c*} = \mathbf{R}^{tw} e_i^c$.

A time-integration procedure for the constitutive equations has been developed, details of which may be found in Staroselsky (1998). The constitutive equations and the time-integration procedure have been implemented in the finite-element program ABAQUS/Explicit (2001) by writing a “user material” subroutine. The polycrystal calculations shown in the following sections have been carried out by modeling each grain as a single finite element.⁸ A set of crystal orientations which approximate the initial crystallographic texture of the material will be assigned to the elements. The macroscopic stress-strain responses will be calculated as volume averages over the entire aggregate.

4. Mechanical behavior of initially-textured magnesium alloy AZ31B

To examine different states of initial crystallographic texture, magnesium alloy AZ31B (96.486% Mg, 2.798% Al, 0.715% Zn, Balance, Mn, Fe) was obtained in two different forms (i) hot-extruded rods, and (ii) hot-rolled plate. We consider these two starting materials separately.

4.1. Initially-textured rod

Experimental measurements of crystallographic texture of the as-received AZ31B rods were carried out by X-ray irradiation using a Rigaku RU 200 diffractometer. Pole figures were obtained by using the Schultz reflection method with copper-K radiation. Partial pole figures were generated by using the Schulz slit on (0001),

⁸ We recognize that a one grain-one element approach may be questionable since it imposes high interaction stresses between grains in order to maintain compatibility. However, the computational resources available to us at this time preclude a more sophisticated three-dimensional polycrystal calculation in which multiple elements represent a single grain.

$\{10\bar{1}0\}$, $\{10\bar{1}1\}$, and $\{11\bar{2}0\}$ crystallographic planes. To process the experimental pole figure data, the Preferred Orientation Package (Kallend et al., 1994) was employed. Each measured pole figure was corrected for background and defocusing, and also extrapolated for the outer 15° . The experimentally-measured (0001) and $\{10\bar{1}0\}$ pole figures are shown in Fig. 4a. Note that the reasonably high intensity of the $\{10\bar{1}0\}$ prismatic planes indicates that a large fraction of these planes are preferentially aligned perpendicular to the e_3 -axis, which is aligned with the rod axis; thus a large fraction of the (0001) basal planes are preferentially aligned parallel to the rod axis. Fig. 4b shows our numerical approximation of this measured texture using 343 unweighted grain orientations. This numerical data for grain orientations was used in our finite element simulations to be discussed below.

Fig. 5a shows a stress–strain curve from a test performed at room temperature at a constant true strain rate, $2 \times 10^{-4} \text{ s}^{-1}$, on a tensile specimen machined from the initially-textured AZ31B rod; the axis of the cylindrical specimen was parallel to the rod axis. The specimen failed at final strain of approximately 0.16.

To simulate a tension test on the initially-textured polycrystalline magnesium rod, we employed a finite-element model of a polycrystalline aggregate. The model consists of a collection of 343 (cube $7 \times 7 \times 7$) 3-D finite elements (ABAQUS-C3D8R), in which each finite-element represents one crystal.

Numerical experiments were carried out to determine the operative slip systems, and the values of the material parameters for the inelastic deformation mechanisms which provided an adequate match to the experimentally-measured stress–strain curve in tension. In our calculations we used the following values for the elastic moduli from the literature (Simmons and Wang, 1971):

$$C_{11} = 58 \text{ MPa}, \quad C_{12} = 25 \text{ MPa}, \quad C_{13} = 20.8 \text{ MPa}, \quad C_{33} = 61.2 \text{ MPa},$$

$$C_{55} = 16.6 \text{ MPa}.$$

Our numerical experiments show that the slip and twinning systems that were operative in tension were the basal (0001) $\langle 11\bar{2}0 \rangle$, prismatic $\{10\bar{1}0\}$ $\langle 11\bar{2}0 \rangle$, and pyramidal $\{10\bar{1}1\}$ $\langle 11\bar{2}0 \rangle$ slip systems, as well as the pyramidal $\{10\bar{1}2\}$ $\langle \bar{1}011 \rangle$ twinning systems.⁹ A set of material parameters that gave an acceptable match to the stress–strain curve is

$$s_{\text{basal}} = 0.55 \text{ MPa}, \quad s_{\text{prismatic}} = 105 \text{ MPa}, \quad s_{\text{pyramidal}} = 105 \text{ MPa}, \quad (20)$$

$$s_{\text{twin}} = 18 \text{ MPa},$$

⁹ A representative optical micrograph exhibiting profuse twinning in our magnesium alloy is shown in Fig. 6. Note that this micrograph does not correspond to that for a specimen after a tension test, but after a plane strain compression experiment to be described in Section 4.2.

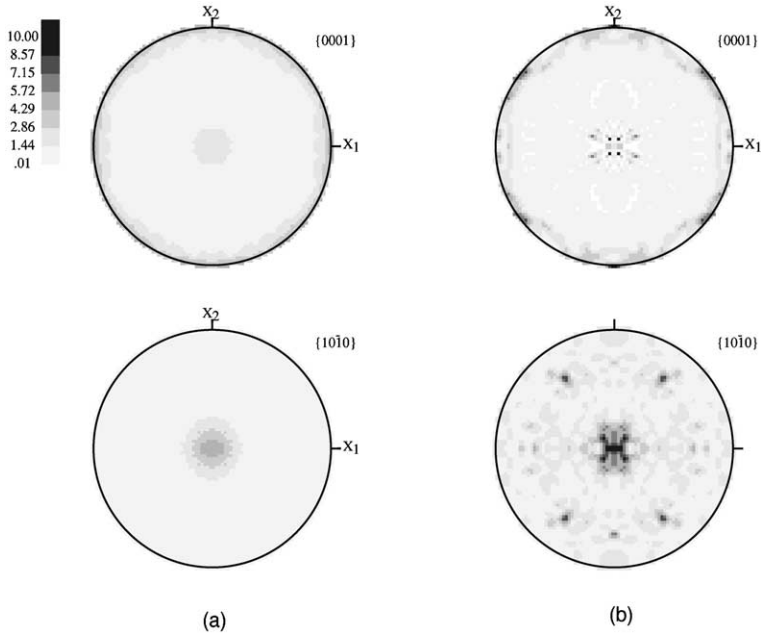


Fig. 4. (a) Experimentally measured initial texture of Mg rod. (b) Numerical representation using 343 crystal orientations.

for the intergranular slip and twin mechanisms,¹⁰ and

$$s_{\text{th}} = 170 \text{ MPa}, \quad s = 220 \text{ MPa}, \quad \dot{\epsilon}_0 = 0.001 \text{ s}^{-1}, \quad m = 0.07, \quad \xi = 0.05, \quad (21)$$

for our simple “isotropic model” for grain boundary accommodation. The quality of curve-fit is shown in Fig. 5(A).

The experimentally measured $\{0001\}$ and $\{10\bar{1}0\}$ pole figures for simple tension after 15% strain are shown in Fig. 5(B)(a). The corresponding numerically-predicted pole figures are shown in Fig. 5(B)(b). Note that, relative to the initial texture, Fig. 4, the intensity of the $\{10\bar{1}0\}$ poles corresponding to the prism planes increased rapidly after a strain of only 15%; these planes are now more nearly aligned perpendicular to the tensile axis, while the basal $\{0001\}$ planes are more nearly parallel to the tensile axis. The qualitative agreement between the numerically-predicted pole figures and the experimental measurements is very good.

We see from the simulations that a non-hardening crystal plasticity model is able to reproduce both the stress–strain response and texture evolution in simple tension. Having estimated the initial texture and the necessary material parameters in the

¹⁰ Note that the slip resistances for the prismatic and pyramidal systems are much higher than the resistance of the basal systems, 105 versus 0.55 MPa. Our numerical experiments show that (a) a variation of slip resistance of the pyramidal systems somewhat influences the stress–strain curve: a change in the value of $s_{\text{pyramidal}}$ from 95 to 120 MPa causes the overall stress response to increase by about 10%, while (b) a variation of the slip resistance for the prismatic systems, $s_{\text{prismatic}}$, does not significantly influence the stress–strain curve for a similar change from 95 to 120 MPa.

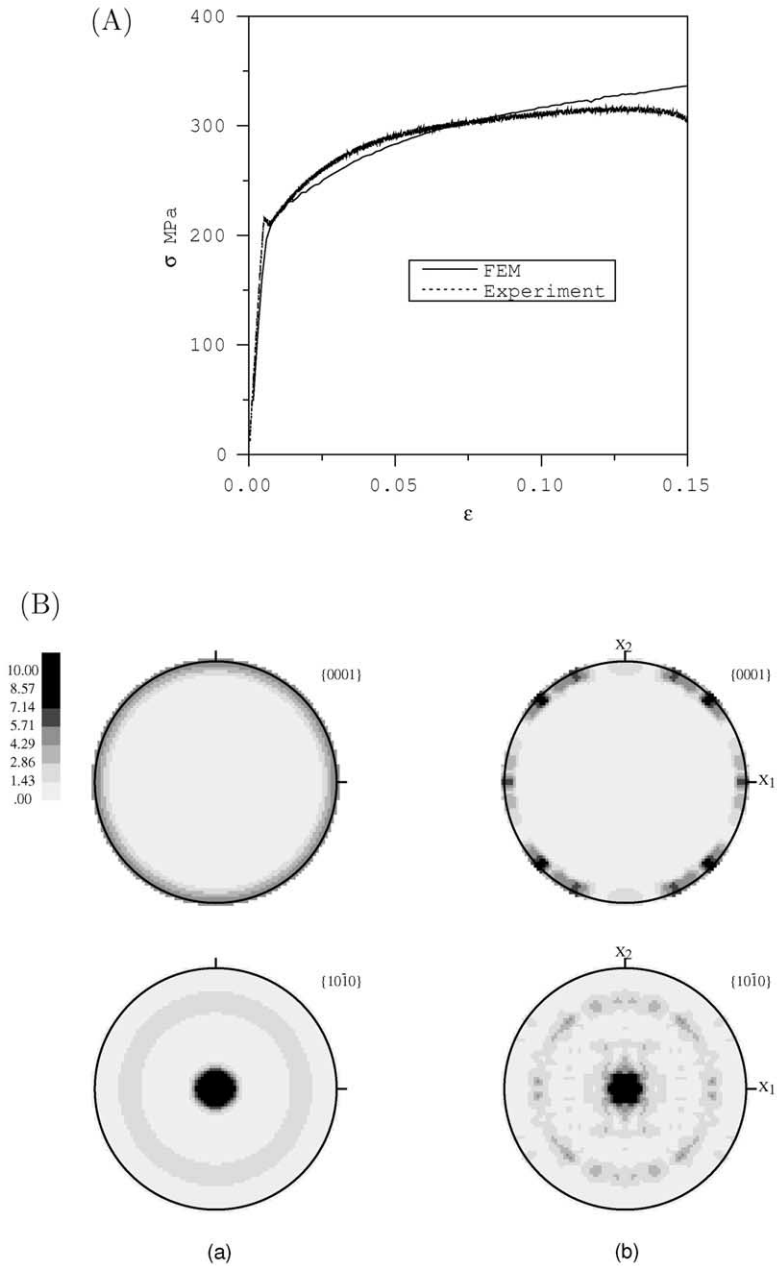


Fig. 5. (A) Comparison of experimentally measured and numerically simulated stress–strain curve in tension for an AZ31B rod. (B) Comparison of (a) experimentally measured and (b) numerically simulated crystallographic textures in simple tension of an AZ31B rod at a tensile strain of 15%.

model, we investigated the predictive capabilities of the model for simple compression of cylindrical specimens made from the rod. The compression experiments were performed to final true strain about 0.18, at which stage the samples fractured. The experimentally-measured and numerically-predicted (i) stress–strain curves are shown in Fig. 7A, and (ii) pole figures are shown in Fig. 7B. The correlation between the predictions and the experimental measurements is very high.

Comparing Figs. 5A and 7A, we note a strong tension-compression asymmetry, which has previously been reported in the literature (e.g., Fig. 6 of Reed-Hill, 1973). Yielding in compression occurs at a stress level which is almost three times smaller than that in tension. As noted previously, this strong tension-compression asymmetry should strongly influence how magnesium and many of its alloys are used as structural members. We emphasize that our numerical simulations have been performed by using a non-hardening plasticity model. The observed strain hardening is related to the evolution of the crystallographic texture.

A comparison of Figs. 4 and 7B shows that the initial texture which had the prismatic $\{10\bar{1}0\}$ planes somewhat aligned perpendicular to the axis of the specimen, quickly gives way to a texture in which the basal (0001) planes become perpendicular to the axis of compression. The initial crystallographic texture of the specimen



Fig. 6. Optical photomicrograph of AZ31B after being deformed in plane strain compression to 18% strain. Note the profuse amount of twinning.

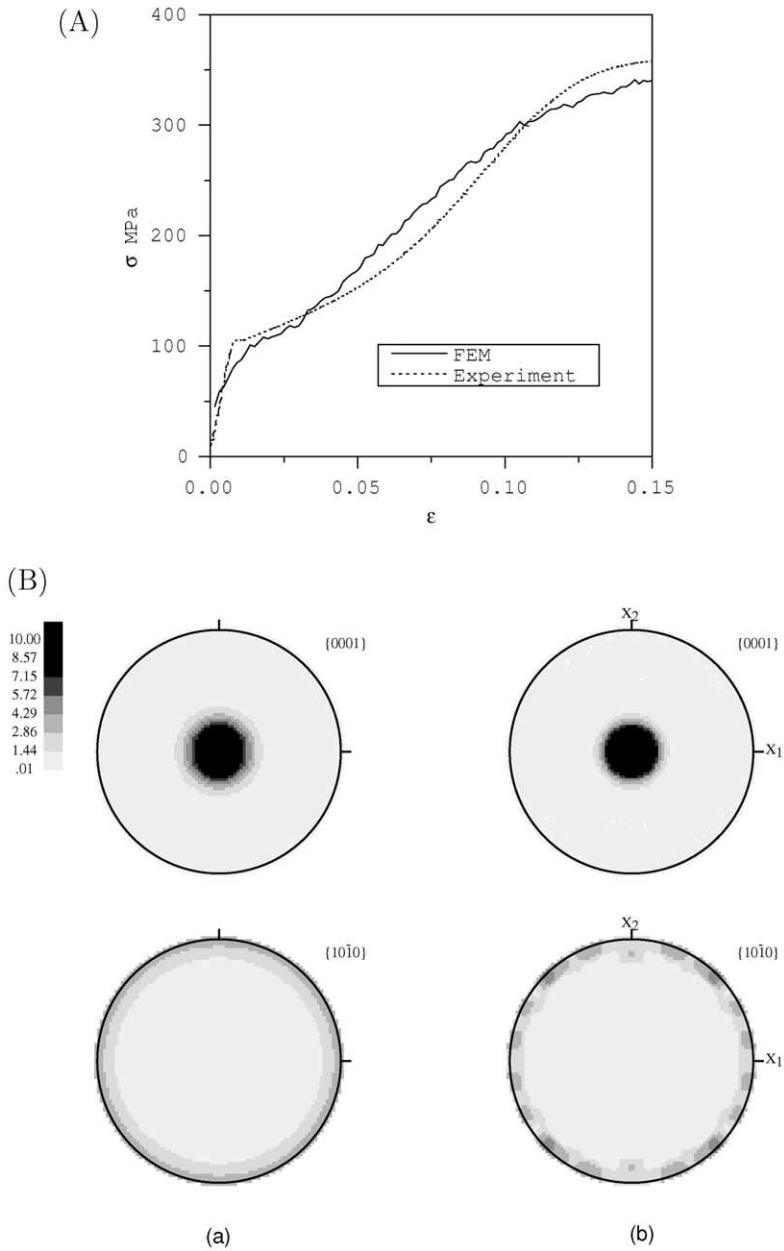


Fig. 7. (A) Comparison of experimentally measured and numerically simulated stress–strain curve in compression for a specimen made from a rod of AZ31B. (B) Comparison of (a) experimentally measured and (b) numerically simulated pole figures after a compressive strain of 18% in specimens made from a rod of AZ31B.

and the compressive mode of deformation are favorable for active basal slipping and deformation twinning. We note that twinning is much more operative in compression than in tension, and this has been confirmed by optical microscopy (Staroselsky, 1998). In compression, the pyramidal- $\langle a \rangle$ slip systems become active when the grains align their $\langle c \rangle$ axis along the compression direction, and the resolved shear stress on the basal plane becomes negligible.

4.2. Initially-textured plate

Let RD, TD and ND denote the rolling direction, transverse direction, and the normal direction of the plate, respectively. The experimentally-measured pole figures are shown in Fig 8a. The high intensity of the $\{0001\}$ basal planes indicates that a large fraction of these planes are preferentially aligned perpendicular to the the normal direction ND of the plate. Fig. 8b shows our numerical approximation of this measured texture using 343 unweighted grain orientations. This numerical data for grain orientations was used in our finite element simulations to be discussed below.

We conducted plane strain compression experiments on specimens machined from the initially-textured plate. The specimens were made almost cubical in shape, and were well-lubricated on all four contact surfaces inside the channel-die plane strain compression fixture.

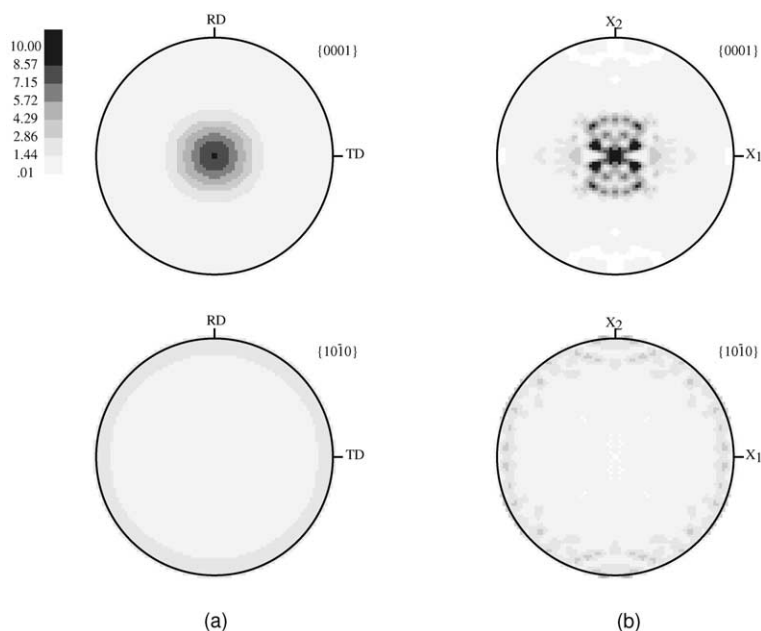


Fig. 8. (a) Experimentally measured initial texture of AZ31B plate. (b) Numerical representation using 343 crystal orientations.

The first set of experiments were conducted with the TD direction of the plate as the plane strain constraint direction, and the ND direction of the plate as the compression direction. Fig. 9 shows a stress–strain curve from such a test.

To simulate a plane strain compression test on the initially-textured polycrystalline magnesium plate, we employed a finite-element consisting of a collection of 343 (cube $7 \times 7 \times 7$) 3-D finite elements (ABAQUS-C3D8R). As before, the macroscopic stress–strain responses are calculated as volume averages over the entire aggregate.

Fig. 9A shows a comparison of the experimentally measured and the numerically fit stress–strain curve. In obtaining the fit, the values of the material parameters for the intragranular mechanisms used were identical to those used in simulating the rod material, Eq. (20), while those for the intergranular mechanism were slightly different, with

$$s_{th} = 210 \text{ MPa}, \quad s = 295 \text{ MPa}, \quad (22)$$

instead of those listed in Eq. (21).

The experimentally measured pole figures for plane strain compression after 15% strain are shown in Fig. 9(B)(a). The corresponding numerically-predicted pole figures are shown in Fig. 9(B)(b). Note that, relative to the initial texture of the plate, Fig. 8, the intensity of the (0001) poles corresponding to the basal planes only increases slightly, and there is no major texture evolution.

Having estimated the initial texture and the necessary material parameters in the model for the plate material, we investigated the predictive capabilities of the model for plane strain compression experiments in which the TD direction of the plate was again the plane strain constraint direction, but this time the RD direction of the plate was the compression direction. The experimentally-measured and numerically-predicted (i) stress–strain curves are shown in Fig. 10A, and (ii) pole figures are shown in Fig. 10B. One can see that the calculated results qualitatively capture the main features of the experimental data. The calculated stress-strain curves resemble experimental relations, but in comparison to the experimental data, the stress level increases more quickly with strain. However, the overall correlation between the predictions and the experimental measurements is very encouraging.

5. Concluding remarks

A crystal-mechanics-based model for the inelastic deformation of hcp metals deforming by slip and twinning has been developed and implemented in the finite-element program ABAQUS/Explicit (2001). We have performed a series of experiments to measure the stress-strain response and texture evolution of the initially-textured polycrystalline magnesium alloy AZ31B under some different modes of deformation. The stress–strain curves and texture evolution predicted by the constitutive model and computational procedures are in reasonable agreement with the experimental measurements.

Our calculations show that the dominant intragranular crystallographic mechanisms are (i) slip on basal (0001) $\langle 11\bar{2}0 \rangle$ and pyramidal $\{10\bar{1}1\}$ $\langle 11\bar{2}0 \rangle$ systems, and (ii)

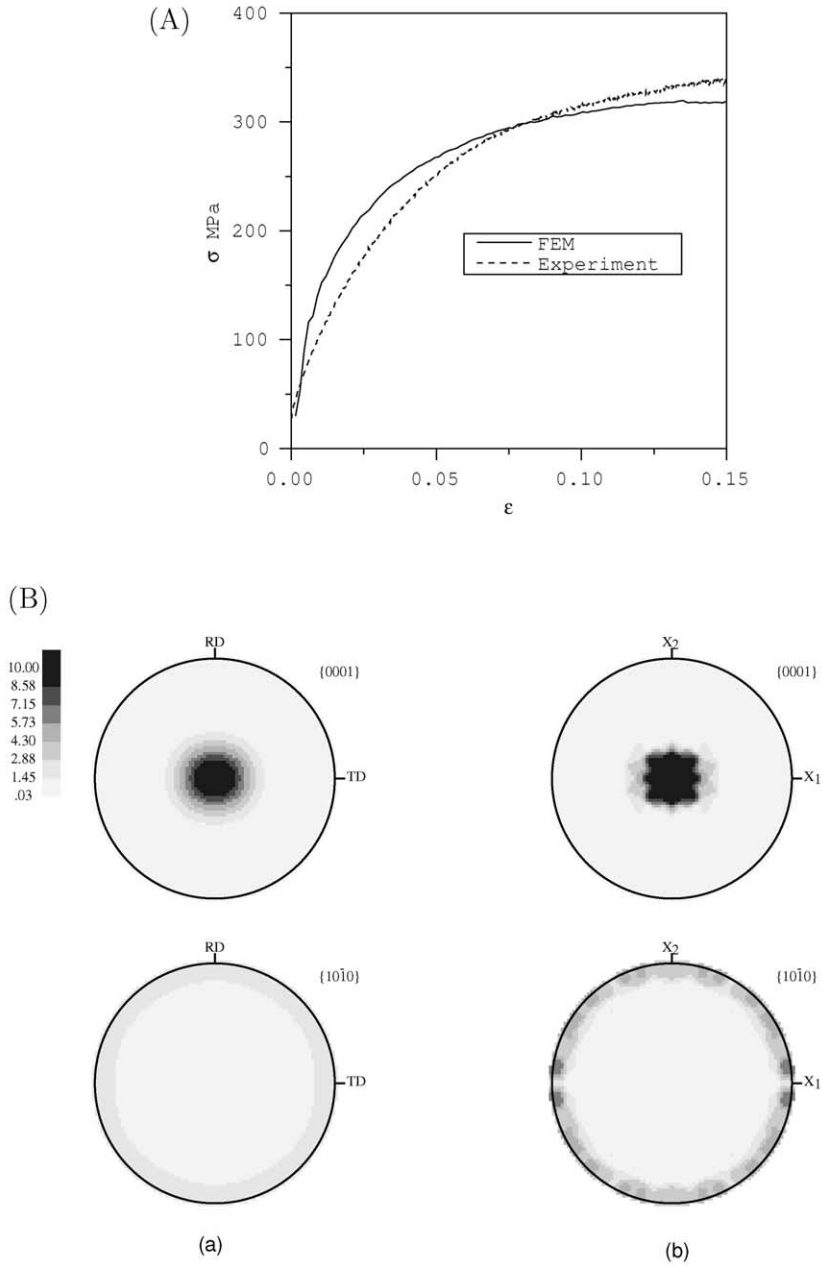


Fig. 9. (A) Comparison of experimentally measured and numerically simulated stress–strain curves in plane strain compression. (B) Comparison of experimentally measured and numerically simulated pole figures in plane strain compression after a strain of 20%. Constraint direction—TD, Compression direction—ND.

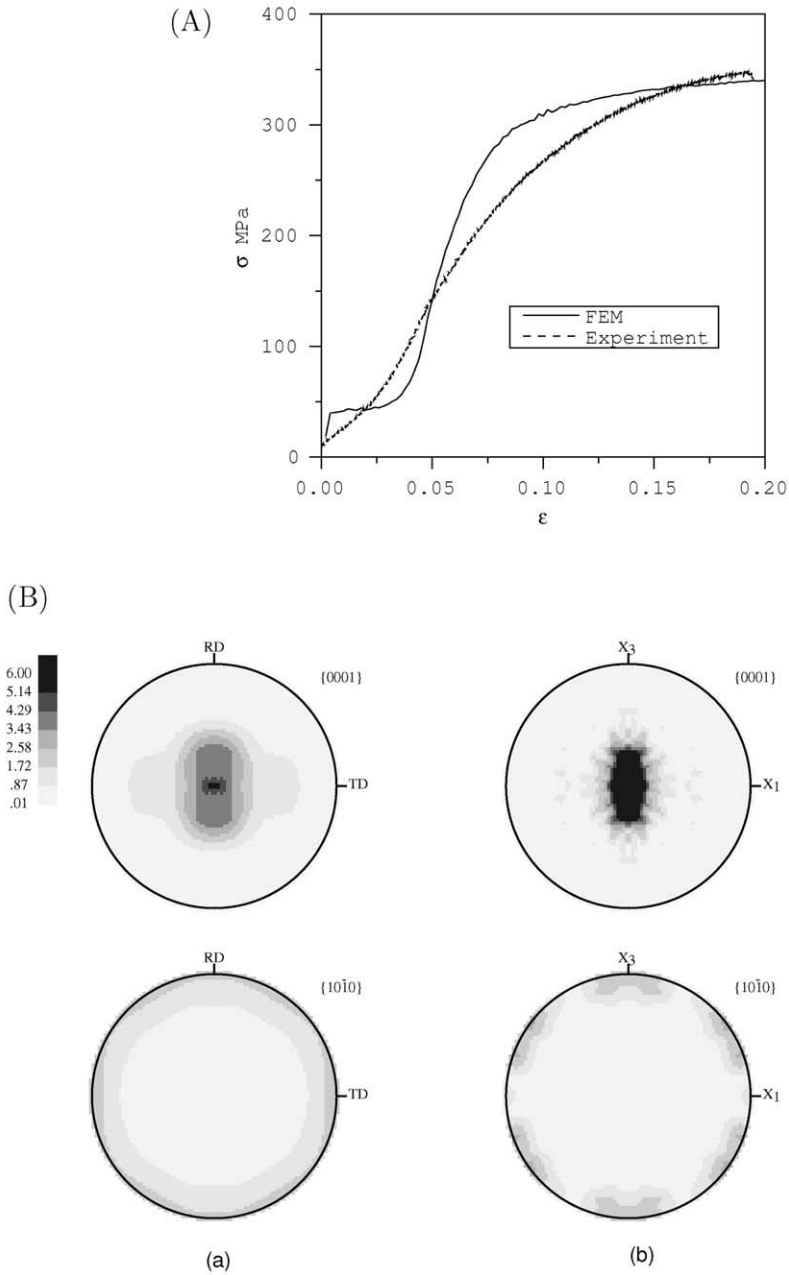


Fig. 10. (A) Comparison of experimentally measured and numerically simulated stress–strain curves in plane strain compression. (B) Comparison of (a) experimentally measured and (b) numerically simulated pole figures after 20% strain in plane strain compression. Constraint direction—TD, Compression direction—RD. 25.

twinning on pyramidal $\{10\bar{1}2\}$ $\langle\bar{1}011\rangle$. The important intergranular grain boundary accommodation effects were accounted for in an approximate fashion by adding a suitably weighted isotropic term to the flow rule; this term serves the important function of bounding the stress levels in the numerical calculations. The strain hardening of the polycrystal is attributed primarily to crystal lattice reorientation during deformation. Our simulations show that the most important mechanism of rapid crystal lattice reorientation is mechanical twinning.

The combined theoretical-numerical-experimental study of initially-textured polycrystalline magnesium reported here, represents a first attempt at a difficult and important topic of deformation in HCP systems; it holds substantial promise for future work for further refinement. In particular, the model needs to be modified to more accurately account for the grain boundary accommodation effects. A proper accounting of these effects requires each crystal to be discretized into a number of subregions in order to capture the gradients in deformation typically expected in the crystals of polycrystalline hcp materials, as well as appropriate traction-displacement interface equations which model the grain boundary sliding/separation phenomena.

Uncited references

Refs. [12,13] are not cited.

Acknowledgements

This work was performed while A. Staroselsky was at MIT, and it was financially supported by the National Science Foundation under Grants CMS9610130 and CMS0002930 to MIT. The ABAQUS finite-element software was made available under an academic license from HKS, Inc. Pawtucket, R.I. The technical help of Srihari Balasubramanian and Maxim Seleznev is gratefully acknowledged.

References

- ABAQUS Reference Manuals, 2001. Pawtucket, R.I.
- Anand, L., Balasubramanian, S., Kothari, M., 1997. Constitutive modelling of polycrystalline metals at large strains. In: Teodosiu, C. (Ed.), *Large Deformation of Crystalline Aggregates*. CISM Courses and Lectures No. 376. Springer, pp. 109–172.
- Balasubramanian, S., Anand, L., 2002. Elasto-viscoplastic constitutive equations for polycrystalline fcc metals at low homologous temperatures. *Journal of the Mechanics and Physics of Solids* 50, 101–126.
- Burke, E.C., Hibbard, W.R., 1952. Plastic deformation of magnesium single crystals. *Transactions of AIME* 194, 295–303.
- Chin, G., Mammel, W., 1970. Competition among basal, prism, and pyramidal slip modes in hcp metals. *Metallurgical Transactions A* 1, 357–361.
- Chin, G.Y., 1975. Development of deformation textures. In: Argon, A.S. (Ed.), *Constitutive Equations in Plasticity*. pp. 431–477.

- Chin, G.Y., Hosford, W.F., Mendorf, D.R., 1969. Accommodation of constrained deformation in f.c.c. metals by slip and twinning. *Proceedings of The Royal Society A* 309, 433–456.
- Christian, J.W., Mahajan, S., 1995. Deformation twinning. *Progress in Materials Science* 39, 1–157.
- Dawson, P.R., Marin, E.B., 1998. Computational mechanics for metal deformation processes using polycrystal plasticity. *Advances in Applied Mechanics* 34, 77.
- Hauser, F.E., Starr, C.D., Tietz, L., Dorn, J.E., 1955. Deformation mechanisms in polycrystalline aggregates of magnesium. *Transactions of ASM* 47, 102–134.
- Hosford, W.G., 1993. *The Mechanics of Crystals and Textured Polycrystals*. Oxford University Press.
- Kalidindi, S.R., 1998. Incorporation of deformation twinning in crystal plasticity models. *Journal of the Mechanics and Physics of Solids* 46, 267–290.
- Kalidindi, S.R., 2001. Modeling anisotropic strain hardening and deformation textures in low stacking fault energy materials. *International Journal of Plasticity* 17, 837–860.
- Kallend, J., Kocks, U., Rollett, A., Wenk, J., 1994. popLA: the Preferred Orientation Package from Los Alamos.
- Kelly, A., Groves, G.W., 1970. *Crystallography and Crystal Defects*. Addison-Wesley.
- Kothari, M., Anand, L., 1998. Elasto-viscoplastic constitutive equations for polycrystalline metals: application to tantalum. *Journal of the Mechanics and Physics of Solids* 46, 51–83.
- Kroner, E., 1960. Allgemeine Kontinuumstheorie der Versetzungen und Eigenspannungen. *Archive for Rational Mechanics and Analysis* 4, 273–334.
- Lee, E.H., 1969. Elastic plastic deformation at finite strain. *ASME Journal of Applied Mechanics* 36, 1–6.
- Myagchilov, S., Dawson, P.R., 1999. Evolution of texture in aggregates of crystals exhibiting both slip and twinning. *Modelling and Simulation in Materials Science and Engineering* 7, 975–1004.
- Pitteri, M., 1985. On the kinematics of mechanical twinning in crystals. *Archives for Rational Mechanics and Analysis* 88, 25–57.
- Pitteri, M., 1986. On type-2 twins in crystals. *International Journal of Plasticity* 2, 99–106.
- Raynor, G.V., 1959. *The Physical Metallurgy of Magnesium and its Alloys*. Pergamon Press.
- Reed-Hill, R.E., 1973. Role of deformation twinning in determining the mechanical properties of metals. In: *The Inhomogeneity of Plastic Deformation*. American Society For Metals, pp. 285–311.
- Schoenfeld, S.E., Kad, B., 2002. Texture effects on shear response in Ti-6Al-4V plates. *International Journal of Plasticity* 18, 461–486.
- Simmons, G., Wang, H., 1971. *Single Crystal Elastic Constants and Calculated Aggregate Properties*. The M.I.T. Press, Cambridge.
- Staroselsky, A., 1998. *Crystal Plasticity due to slip and Twinning*. Doctoral dissertation, Massachusetts Institute of Technology.
- Staroselsky, A., Anand, L., 1998a. Inelastic Deformation of F.C.C. Materials by Slip and Twinning. *Journal of the Mechanics and Physics of Solids* 46, 671–696.
- Staroselsky, A., Anand, L., 1998b. Inelastic deformation of fcc single crystals by slip and twinning. In: de Borst, R., van der Giessen, E. (Eds.), *Material Instabilities in Solids*. John Wiley, pp. 227–242.
- Tome, C., Lebhenson, R.A., Kocks, U.F., 1978. A model for texture development dominated by deformation twinning: application to zirconium alloys. *Acta Metallurgica* 39, 2667–2680.
- Van-Houtte, P., 1978. Simulation of the rolling and shear texture of brass by the Taylor theory adapted for mechanical twinning. *Acta Metallurgica* 26, 591–604.
- Zanzotto, G., 1996. The cauchy-born hypothesis, nonlinear elasticity and mechanical twinning in crystals. *Acta Crystallographica Section A* A52, 839–849.